Université de Mons
Faculté Polytechnique – Service de Mécanique Rationnelle, Dynamique et Vibrations
31, Bld Dolez - B-7000 MONS (Belgique)
065/37 42 15 – georges.kouroussis@umons.ac.be

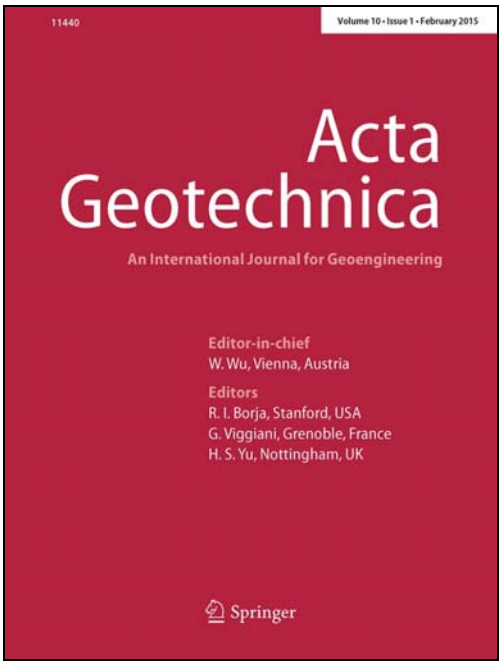

L. Qu, C. Yang, X. Ding, G. Kouroussis, C. Zheng, A continuum-based model on axial pile-head dynamic impedance in inhomogeneous soil, *Acta Geotechnica*, 16(10), 3339–3353, 2021.

Acta Geotechnica (2021) 16:3339–3353
https://doi.org/10.1007/s11440-021-01274-x

RESEARCH PAPER

A continuum-based model on axial pile-head dynamic impedance in inhomogeneous soil

Liming Qu[1] · Changwei Yang[1] · Xuanming Ding[2] · Georges Kouroussis[3] · Changjie Zheng[4,5]

Received: 11 February 2021 / Accepted: 12 June 2021 / Published online: 2 July 2021

Abstract
This paper presents a closed-form solution on the steady dynamic response of circular piles embedded in inhomogeneous soil. The soil is modeled as a viscoelastic continuum, and the pile is modeled as a one-dimensional elastic shaft. Fictitious soil pile model and Hamilton's energy principle are introduced to deduce the equations governing the layered pile–soil system. Impedance transfer method and iterative algorithm are deduced to decouple the pile–soil dynamic interaction. The results show that the modulus and thickness of inhomogeneous soil profile play a more significant role in the dynamic stiffness than the damping effects. The variation pattern of the dynamic impedance against the modulus of layered soil is dominated by the cut-off frequency. Particularly, in Gibson soil, the stiffer surface soil yields the greater pile-head stiffness. The dynamic stiffness of piles in Gibson soil could be approximated by two or more soil layers with equivalent Young's modulus.

Keywords Dynamic impedance · Fictitious soil pile · Hamilton's energy principle · Inhomogeneous soil · Piles

1 Introduction

The model of beam-on-dynamic-Winkler-foundation (BDWF) [2, 5, 23] is a widely used method to analyze the dynamic responses of pile-supported superstructures such as bridges, buildings, transmission tower, oil drilling platforms. To obtain the required Winkler coefficients in BDWF model, the pile-head dynamic impedance should be accurately calculated. It is well admitted that the mechanical behaviors of piles rely on their interaction with surrounding soil [4, 7, 8, 10, 16–18, 26]. Voigt model considers the soil resistance as discrete springs and damping spots around a pile [19, 20], which means the coupled pile–soil vibration is neglected. Moreover,

✉ Changwei Yang
1209732335@qq.com

Liming Qu
hustqlm@163.com

Xuanming Ding
dxmhhu@163.com

Georges Kouroussis
georges.kouroussis@umons.ac.be

Changjie Zheng
zhengchj1989@163.com

[1] MOE Key Laboratory of High-Speed Railway Engineering, College of Civil Engineering, Southwest Jiaotong University, Chengdu 610031, China

[2] Key Laboratory of New Technology for Construction of Cities in Mountain Area, College of Civil Engineering, Chongqing University, Chongqing 400045, China

[3] Department of Theoretical Mechanics, Dynamics and Vibrations, Faculty of Engineering, Université de Mons, Mons, Belgium

[4] School of Civil Engineering, Fujian University of Technology, Fuzhou 350118, China

[5] Fujian Provincial Key Laboratory of Advanced Technology and Informatization in Civil Engineering, Fuzhou 350118, China

conventional Voigt model requires intricate calibration process to determine the parameters of springs and damping spots, which significantly affect the calculated results and the applicability of the approach. Novak [15] proposed a plane strain method accounting for the vertical pile–soil interaction by treating the soil as independent and infinitely thin layers. However, neglecting the mechanical interaction among soil layers makes that the plane strain model could solely capture the horizontal wave propagation in soil. Wu et al. [25] introduced the Voigt model to formulate the stress transfer between adjacent soil layers to investigate the influences of soil anisotropy on the velocity admittance at the pile head. Their results showed that soil modulus variation in the vertical plane caused more notable influence than that in the horizontal plane. Cui et al. [1] formulated the dynamic impedance of floating piles in saturated soil by assuming the pile base soil as spring-dashpot elements. Zheng et al. [29] and Gan et al. [6] analytically studied the vertical vibration of piles in half-space and finite-thickness soil layer, respectively. In their studies, the soil beneath the pile tip is treated as a homogeneous continuum, whereas the surrounding soil adopts the plane strain assumption. By modeling the whole pile–soil system as a continuum and taking the vertical stress gradient and radial displacement into consideration, Zheng et al. [28] deduced a rigorous analytical solution for the vertical dynamic impedance of end-bearing piles in homogeneous soil. They found that the dynamic stiffness was underestimated at low frequency range under the plane strain assumption of surrounding soil. In addition, two cut-off frequencies were obtained in Zheng et al. [28], which indicated the resonance of shear waves and longitudinal waves in soil. In contrast, the solution method based on plane strain model did not reflect any cut-off frequency. Using the extended Hamilton's principle in continuum mechanics, Gupta and Basu [3] developed a relatively convenient method for the vertical dynamic response of piles in a homogeneous soil. Since the radial displacement was ignored, Gupta and Basu's method only predicted one cut-off frequency but did not bring significant difference from the rigorous analytical technique. However, studies on the effects of inhomogeneous soil profile on the dynamic impedance based on the continuum model are far from sufficient.

This paper presents a closed-form solution for the vertical dynamic impedance of piles in inhomogeneous soil. The motion of the pile–soil continuum system is formulated by the product of pile displacement and a decay function. A variational analysis is used to deduce the governing dynamic equations. Impedance transfer method [11, 27] and iterative technique (Seo et al.) [22] are used to decouple the dynamic pile–soil interaction in layered soil. The present solution is compared with existing analytical solutions to validate its feasibility. Finally, the effects of inhomogeneous deposit profile on the dynamic stiffness and damping of piles are examined in layered soil and Gibson type of soil, respectively.

2 Problem definition

A circular pile is considered, embedded in a horizontally layered soil as illustrated in Fig. 1. The pile has a Young's modulus E_p, a density ρ_p, a diameter $2r_p$, a cross-section area A_p and a length L. The soil profile contains a total of N layers with M layers around the pile shaft and N-M layers below the pile tip. The pile–soil system is assumed as a linear continuum, and no physical slippage could occur at pile–soil interface. The soil behavior is viscoelastic with a hysteretic damping ratio β_0, a Young's modulus E_s, a Poisson's ratio of υ_s and a density ρ_s. The soil column beneath the pile tip is modeled by a fictitious soil pile. For the dynamic analysis, complex forms of Young's modulus, shear modulus and Lame's constant are introduced as $E_s^* = E_s(1 + 2i\beta_0)$, $G_s^* = E_s^*/[2(1+\upsilon_s)]$ and $\lambda_s^* = E_s^*\upsilon_s/[(1+\upsilon_s)(1-2\upsilon_s)]$, respectively. The pile head is subjected to a harmonic force $F(t) = F_0 e^{i\omega t}$ at the vertical direction, where F_0 denotes the force amplitude, ω represents the force frequency, t and i are time and the imaginary unit, respectively. The objective of this study is to analyze the effects of inhomogeneous soil profile on the dynamic impedance of piles subjected to axial loads.

3 Displacement model

Figure 2 depicts the displacement components of a pile–soil system and the stress components of a soil element in the cylindrical coordinates. The radial displacement u_r and

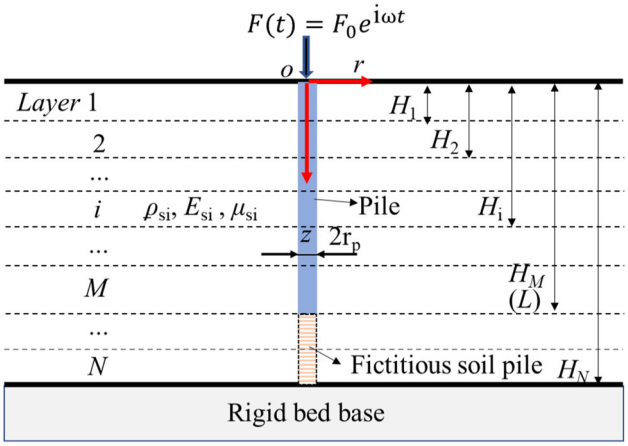

Fig. 1 Axially loaded circular pile embedded in layered soil

circumferential displacement u_θ of a pile–soil system are trivial under the vertical load and thus are neglected in this study. The vertical displacement u_z of the pile–soil system is defined as a function of the radial distance r, the depth z and the time t as

$$u_z(r,z,t) = w(z,t)\phi(r) \tag{1}$$

where $w(z,t)$ is equal to the axial displacement of pile shaft $w_p(z,t)$ when $0 \le z \le L$; and when $L < z \le H_N$, $w(z,t)$ represents the vertical displacement of the fricticious soil pile $w_s(z,t)$, so as:

$$w(z,t) = w_p(z,t),\ (z \le L) \tag{2a}$$

$$w(z,t) = w_s(z,t),\ (z > L) \tag{2b}$$

$\phi(r)$ is a dimensionless decay function that is introduced to evaluate the soil displacement attenuation in the radial direction. Since the displacement variation along the pile cross-section ($r \le r_p$) is small, the pile is assumed as one-dimensional shaft and the soil beneath pile tip is treated as a virtual pile. Therefore, $\phi(r)$ should satisfy the following inherent boundary conditions:

$$\phi(r) = \begin{cases} 1, & 0 \le r \le r_p \\ 0, & r \to \infty \end{cases}. \tag{3}$$

The relationship between stress and strain in an elastic soil medium is written as:

$$\begin{bmatrix} \sigma_{zz} \\ \sigma_{rr} \\ \sigma_{\theta\theta} \\ \tau_{rz} \\ \tau_{z\theta} \\ \tau_{r\theta} \end{bmatrix} = \begin{bmatrix} \lambda_s^* + 2G_s^* & \lambda_s^* & \lambda_s^* & 0 & 0 & 0 \\ \lambda_s^* & \lambda_s^* + 2G_s^* & \lambda_s^* & 0 & 0 & 0 \\ \lambda_s^* & \lambda_s^* & \lambda_s^* + 2G_s^* & 0 & 0 & 0 \\ 0 & 0 & 0 & G_s^* & 0 & 0 \\ 0 & 0 & 0 & 0 & G_s^* & 0 \\ 0 & 0 & 0 & 0 & 0 & G_s^* \end{bmatrix} \begin{bmatrix} \varepsilon_{zz} \\ \varepsilon_{rr} \\ \varepsilon_{\theta\theta} \\ \gamma_{rz} \\ \gamma_{z\theta} \\ \gamma_{r\theta} \end{bmatrix}. \tag{4}$$

The relationship between displacement and strain is given by:

$$\begin{bmatrix} \varepsilon_{zz} \\ \varepsilon_{rr} \\ \varepsilon_{\theta\theta} \\ \gamma_{rz} \\ \gamma_{z\theta} \\ \gamma_{r\theta} \end{bmatrix} = \begin{bmatrix} -\dfrac{\partial u_z}{\partial z} \\ -\dfrac{\partial u_r}{\partial r} \\ -\dfrac{u_r}{r} - \dfrac{1}{r}\dfrac{\partial u_\theta}{\partial \theta} \\ -\dfrac{\partial u_z}{\partial r} - \dfrac{\partial u_r}{\partial z} \\ -\dfrac{1}{r}\dfrac{\partial u_z}{\partial \theta} - \dfrac{\partial u_\theta}{\partial z} \\ -\dfrac{1}{r}\dfrac{\partial u_r}{\partial \theta} - \dfrac{\partial u_\theta}{\partial r} + \dfrac{u_\theta}{r_\theta} \end{bmatrix} = \begin{bmatrix} -\phi(r)\dfrac{\partial w}{\partial z} \\ 0 \\ 0 \\ -w\dfrac{\partial \phi(r)}{\partial r} \\ 0 \\ 0 \end{bmatrix}. \tag{5}$$

Substituting Eq. (5) into Eq. (4), the strain energy density in soil υ_{soil} can be expressed as:

$$\begin{aligned} \upsilon_{soil} &= (\sigma_{zz}\varepsilon_{zz} + \sigma_{rr}\varepsilon_{rr} + \sigma_\theta\varepsilon_\theta + \tau_{rz}\gamma_{rz} + \tau_{z\theta}\gamma_{z\theta} + \tau_{r\theta}\gamma_{r\theta})/2 \\ &= \frac{1}{2}\left((\lambda_s^* + 2G_s^*)\left(\phi\frac{\partial w_s}{\partial z}\right)^2 + G_s^* w_s^2 \left(\frac{\partial \phi(r)}{\partial r}\right)^2 \right). \end{aligned} \tag{6}$$

Similarly, the strain energy density in pile υ_{pile} can be expressed as:

$$\upsilon_{pile} = \frac{1}{2}E_p A_p \left(\frac{\partial w_p}{\partial z}\right)^2 \tag{7}$$

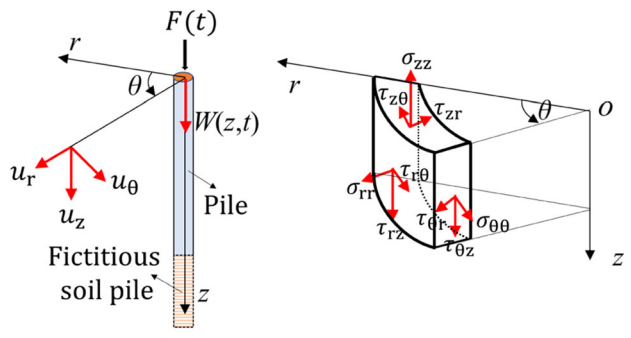

(a) Displacement **(b)** Stress component of a soil element

Fig. 2 Displacement and stress components for a pile–soil system in cylindrical coordinates

4 Energy formations and Hamilton's principle in a pile–soil system

For a vibrating pile–soil system, the total energy ($\Re$) includes the kinetic energy T, the potential energy U and the work W made by external forces. Integrating the energy in pile shaft and all soil layers, these three types of energy components are given by the following:where H_i is the depth of the ith soil layer (subscripts i and j indicate each layer for displacement $w_{\mathrm{p}i}$ and $w_{\mathrm{s}j}$).

$$\begin{aligned} T &= T_{\mathrm{pile}} + T_{\mathrm{soil}} \\ &= \sum_{i=1}^{M}\left[\int_{H_i}^{H_{i+1}} \frac{1}{2}\rho_{\mathrm{p}}A_{\mathrm{p}}\left(\frac{\partial w_{pi}}{\partial t}\right)^2 \mathrm{d}z + \int_{H_i}^{H_{i+1}}\int_{0}^{2\pi}\int_{r_{\mathrm{p}}}^{\infty}\frac{1}{2}\rho_{si}\phi^2\left(\frac{\partial w_{pi}}{\partial t}\right)^2 r\mathrm{d}r\mathrm{d}\theta\mathrm{d}z\right] \\ &\quad + \sum_{j=M+1}^{N}\left[\int_{H_j}^{H_{j+1}} \frac{1}{2}\rho_{sj}A_{\mathrm{p}}\left(\frac{\partial w_{sj}}{\partial t}\right)^2 \mathrm{d}z + \int_{H_j}^{H_{j+1}}\int_{0}^{2\pi}\int_{r_{\mathrm{p}}}^{\infty}\frac{1}{2}\rho_{sj}\phi^2\left(\frac{\partial w_{sj}}{\partial t}\right)^2 r\mathrm{d}r\mathrm{d}\theta\mathrm{d}z\right] \end{aligned} \tag{8}$$

$$\begin{aligned} U &= U_{\mathrm{pile}} + U_{\mathrm{soil}} \\ &= \sum_{i=1}^{M}\left[\int_{H_i}^{H_{i+1}} \frac{1}{2}E_{\mathrm{p}}A_{\mathrm{p}}\left(\frac{\partial w_{pi}}{\partial z}\right)^2 \mathrm{d}z + \int_{H_i}^{H_{i+1}}\int_{0}^{2\pi}\int_{r_{\mathrm{p}}}^{\infty}\frac{1}{2}\left(\left(\lambda_s^* + 2G_s^*\right)\phi^2\left(\frac{\partial w_{pi}}{\partial z}\right)^2 + G_s^* w_{pi}^2\left(\frac{\partial \phi(r)}{\partial r}\right)^2\right) r\mathrm{d}r\mathrm{d}\theta\mathrm{d}z\right] \\ &\quad + \sum_{j=M+1}^{N}\left[\int_{H_i}^{H_{i+1}} \frac{1}{2}\left(\lambda_s^* + 2G_s^*\right)A\left(\frac{\partial w_{si}}{\partial z}\right)^2 \mathrm{d}z + \int_{H_j}^{H_{j+1}}\int_{0}^{2\pi}\int_{0}^{\infty}\frac{1}{2}\left(\left(\lambda_s^* + 2G_s^*\right)\left(\phi\frac{\partial w_{si}}{\partial z}\right)^2 + G_s^* w_{si}^2\left(\frac{\partial \phi(r)}{\partial r}\right)^2\right) r\mathrm{d}r\mathrm{d}\theta\mathrm{d}z\right] \end{aligned} \tag{9}$$

$$W = F_0 u_{z=0} \tag{10}$$

Following the Hamilton variational principle, the energy function $\Re$ during the period from t_1 to t_2 of a mechanical system approaches the equilibrium state when the variation of the function $\Re$ gets its minimal value, which yields:

$$\delta\Re = \int_{t_1}^{t_2}(\delta T - \delta U + \delta W)\mathrm{d}t = 0 \tag{11}$$

where $\delta(\bullet)$ denotes the variational operator.

Introducing the steady vibration condition $w(z,t) = w(z)e^{i\omega t}$ in Eq. (8) and substituting Eqs. (8), (9) and (10) into Eq. (11) yield the following equation:

5 Governing equations and solving process

5.1 Pile and the soil column beneath the pile tip

Collecting the coefficients w_{pi} from the variational formula in Eq. (12), the governing equation of a pile subjected to axial loads can be obtained:

$$
\begin{aligned}
\delta\Re = &\sum_{i=1}^{M}\left\{\omega^2\rho_{\mathrm{p}}A_{\mathrm{p}}\int_{t_1}^{t_2}\int_{H_i}^{H_{i+1}} w_p\delta w_p \mathrm{d}t\mathrm{d}z + 2\pi\rho_s\omega^2\int_{t_1}^{t_2}\int_{H_i}^{H_{i+1}}\int_{r_{\mathrm{p}}}^{\infty}\phi^2 w_p\delta w_p r\mathrm{d}r\mathrm{d}z\mathrm{d}t + 2\pi\rho_s\omega^2\int_{t_1}^{t_2}\int_{H_i}^{H_{i+1}}\int_{r_{\mathrm{p}}}^{\infty} r\phi w_p^2\delta\phi\mathrm{d}r\mathrm{d}z\mathrm{d}t\right\}\\
&+\sum_{j=M+1}^{N}\left\{\omega^2\rho_s A_{\mathrm{p}}\int_{t_1}^{t_2}\int_{L}^{\infty} w_s\delta w_s\mathrm{d}t\mathrm{d}z + 2\pi\rho_s\omega^2\int_{t_1}^{t_2}\int_{H_j}^{H_{j+1}}\int_{r_{\mathrm{p}}}^{\infty} r\phi^2 w_s\delta w_s\mathrm{d}r\mathrm{d}z\mathrm{d}t + 2\pi\rho_s\omega^2\int_{t_1}^{t_2}\int_{H_j}^{H_{j+1}}\int_{r_{\mathrm{p}}}^{\infty} r\phi w_s^2\delta\phi\mathrm{d}r\mathrm{d}z\mathrm{d}t\right\}\\
&+\sum_{i=1}^{M}\left\{-E_{\mathrm{p}}A_{\mathrm{p}}\int_{t_1}^{t_2}\left(\frac{\partial w_p}{\partial z}\delta w_p\Big|_{H_i}^{H_{i+1}} - \int_{H_i}^{H_{i+1}}\frac{\partial^2 w_p}{\partial z^2}\delta w_p\mathrm{d}z\right)\mathrm{d}t - \pi\left(\lambda_{si}^* + 2G_{si}^*\right)\int_{t_1}^{t_2}\right.\\
&\left[2\int_{r_{\mathrm{p}}}^{\infty}\left(\frac{\partial w_p}{\partial z}\right)\phi^2 r\delta w_p\Big|_{H_i}^{H_{i+1}} - 2\int_0^L\int_{r_{\mathrm{p}}}^{\infty} r\phi^2\left(\frac{\partial^2 w_p}{\partial z^2}\right)\delta w_p\mathrm{d}r\mathrm{d}z + 2\int_0^L\int_{r_{\mathrm{p}}}^{\infty}\phi\left(\frac{\partial w_p}{\partial z}\right)^2\delta\phi r\mathrm{d}r\mathrm{d}z\right]\mathrm{d}t\\
&-\pi G_s^*\int_{t_1}^{t_2}\left[2\int_{H_i}^{H_{i+1}}\int_{r_{\mathrm{p}}}^{\infty}\left(\frac{\partial\phi}{\partial r}\right)^2 w_p r\delta w_p\mathrm{d}r\mathrm{d}z + 2\int_{H_i}^{H_{i+1}} w_p^2\frac{\partial\phi}{\partial r}r\delta\phi dz\Big|_{r_{\mathrm{p}}}^{\infty} - 2\int_{H_i}^{H_{i+1}}\int_{r_{\mathrm{p}}}^{\infty} w_p^2\left(r\frac{\partial^2\phi}{\partial r^2} + \frac{\partial\phi}{\partial r}\right)\delta\phi\mathrm{d}r\mathrm{d}z\right]\mathrm{d}t\Bigg\}\\
&+\sum_{j=M+1}^{N}\left\{-\left(\lambda_s^* + 2G_s^*\right)A_{\mathrm{p}}\int_{t_1}^{t_2}\left(\frac{\partial w_s}{\partial z}\delta w_s\Big|_{H_j}^{H_{j+1}} - \int_0^L\frac{\partial^2 w_s}{\partial z^2}\delta w_s\mathrm{d}z\right)\mathrm{d}t\right.\\
&-\pi\left(\lambda_{sj}^* + 2G_{sj}^*\right)\int_{t_1}^{t_2}\left[2\int_{r_{\mathrm{p}}}^{\infty}\left(\frac{\partial w_s}{\partial z}\right)\phi^2 r\delta w_s\Big|_{H_j}^{H_{j+1}} - 2\int_{r_{\mathrm{p}}}^{\infty}\int_L^{\infty} r\phi^2\left(\frac{\partial^2 w_s}{\partial z^2}\right)\delta w_s\mathrm{d}z\mathrm{d}r + 2\int_{H_j}^{H_{j+1}}\int_{r_p}^{\infty} r\phi\left(\frac{\partial w_s}{\partial z}\right)^2\delta\phi\mathrm{d}r\mathrm{d}z\right]\mathrm{d}t\\
&-\pi G_s^*\int_{t_1}^{t_2}\left[2\int_{H_j}^{H_{j+1}} w_s^2\left(\frac{\partial\phi}{\partial z}\right)r\delta\phi\mathrm{d}z\Big|_{r_{\mathrm{p}}}^{\infty} - 2\int_{r_{\mathrm{p}}}^{\infty}\int_{H_j}^{H_{j+1}} w_s^2\left(r\frac{\partial^2\phi}{\partial r^2} + \frac{\partial\phi}{\partial z}\right)\delta\phi\mathrm{d}z\mathrm{d}r + 2\int_{H_j}^{H_{j+1}}\int_{r_{\mathrm{p}}}^{\infty} w_s\left(\frac{\partial\phi}{\partial r}\right)^2\delta w_s r\mathrm{d}r\mathrm{d}z\right]\mathrm{d}t\Bigg\} = 0.
\end{aligned}
\tag{12}
$$

$$
\left(E_{\mathrm{p}i}A + t_i\right)\frac{\partial^2 w_{pi}}{\partial z^2} - \left[k_i - (\alpha_i + \rho_{\mathrm{p}i}A)\omega^2\right]w_{pi} = 0. \tag{13}
$$

Similarly, the governing equation of soil beneath the pile bottom can be written:

$$
\left[\left(\lambda_{si}^* + 2G_{si}^*\right)A + 2t_i\right]\frac{\partial^2 w_{si}}{\partial z^2} - \left[k_i - (\alpha_i + \rho_{si}A)\omega^2\right]w_{si} = 0 \tag{14}
$$

where

$$
t_i = \pi\left(\lambda_{si}^* + 2G_{si}^*\right)\int_{r_{\mathrm{p}}}^{\infty}\phi^2 r\mathrm{d}r \tag{15a}
$$

$$
\alpha_i = 2\pi\rho_{si}\int_{r_{\mathrm{p}}}^{\infty}\phi^2 r\mathrm{d}r \tag{15b}
$$

$$
k_i = 2\pi G_{si}^*\int_{r_{\mathrm{p}}}^{\infty}\left(\frac{\partial\phi}{\partial r}\right)^2 r\mathrm{d}r. \tag{15c}
$$

The general solutions of Eq. (13) and Eq. (14) are given by:

$$
w_{pi}(z) = B_{pi}e^{\lambda_{pi}z} + C_{pi}e^{-\lambda_{pi}z},\ (1 \le i \le M) \tag{16a}
$$

$$
w_{si}(z) = B_{si}e^{\lambda_{si}z} + C_{si}e^{-\lambda_{si}z},\ (M+1 \le i \le N) \tag{16b}
$$

where

$$
\lambda_{pi} = \sqrt{\frac{k_i - (\alpha_i + \rho_i A)\omega^2}{E_p A + 2t_i}} \tag{17a}
$$

$$
\lambda_{si} = \sqrt{\frac{k_i - (\alpha_i + \rho_i A)\omega^2}{\left(\lambda_{si}^* + 2G_{si}^*\right)A_p + 2t_i}} \tag{17b}
$$

The solutions in Eqs. (16a) and (16b) for the vibration of a pile and the soil beneath the pile have a similar form. For the sake of simplification, the terms of $\lambda_{si}^{*}+2G_{si}^{*}$ in Eq. (17b) and E_p in Eq. (17a) are expressed in the form of equivalent elastic modulus $\overline{E_i}$, i.e., $\overline{E_i}=E_p,\ (1\le i\le M);\ \overline{E_i}=\lambda_{si}^{*}+2G_{si}^{*},\ (M+1\le i\le N)$. Consequently, Eqs. (16a) and (16b) can be integrated into a unified expression, that is:

$$w_i(z)=B_ie^{\lambda_i z}+C_ie^{-\lambda_i z},\ (1\le i\le N) \tag{18}$$

The axial force $Q_i(z)$ in pile shaft in the ith layer is given by:

$$Q_i(z)=-(E_iA+2t_i)\frac{\partial w_i}{\partial z}=-B_i\zeta_ie^{\lambda_i z}+C_i\zeta_ie^{-\lambda_i z} \tag{19}$$

where

$$\zeta_i=\sqrt{[k_i-(\alpha_i+\rho_iA)\omega^2](E_iA+2t_i)}. \tag{20}$$

The expressions in Eq. (18) and Eq. (19) have 2 N unknown constants (B_1, $B_2\ldots B_i,..B_N$; C_1, $C_2\ldots C_i,..C_N$), which needs 2 N boundary conditions to determine their values. Firstly, the displacement and force between any two adjacent layers should be identical, which gives 2 N-2 boundary conditions as follows:

$$e^{\lambda_iH_i}B_i+e^{-\lambda_iH_i}C_i-e^{\lambda_{i+1}H_i}B_{i+1}-e^{-\lambda_{i+1}H_i}C_{i+1}=0,\ (1\le i\le N-1) \tag{21}$$

$$-\zeta_iB_ie^{\lambda_iH_i}+\zeta_iC_ie^{-\lambda_iH_i}+\zeta_{i+1}e^{\lambda_{i+1}H_i}B_{i+1}-\zeta_{i+1}e^{-\lambda_{i+1}H_i}C_{i+1}=0,\ (1\le i\le N-1). \tag{22}$$

Secondly, the force at the pile head should be equal to the external load, which yields:

$$-B_1\zeta_1e^{\lambda_1 z}+C_1\zeta_1e^{-\lambda_1 z}=F_0. \tag{23}$$

Finally, the vertical soil displacement must be zero on the rigid rock at $z=H_N$, which is given by:

$$w_{si}(z)|_{i=N}=0. \tag{24}$$

Substituting Eq. (18) into Eq. (24), we obtain:

$$\frac{B_N}{C_N}=-e^{-2\lambda_NH_N}. \tag{25}$$

By solving the equations above, the unknown constants can be either analytically or numerically determined. Here, a method through impedance transfer is applied to obtain the explicit solution of B_i and C_i for all the soil layers.

The axial dynamic impedance $K_d(z)$ of a pile and soil column below the pile tip at any depth z from 0 to H can be expressed as:

$$K_d(z)=\frac{-B_i\zeta_ie^{\lambda_i z}+C_i\zeta_ie^{-\lambda_i z}}{B_ie^{\lambda_i z}+C_ie^{-\lambda_i z}},\ (1\le i\le N). \tag{26}$$

Since the dynamic impedances at any adjacent layers are identical, the following equation can be written:

$$\frac{B_i}{C_i}=\frac{-\frac{B_{i+1}}{C_{i+1}}\left(\frac{\zeta_{i+1}}{\zeta_i}+1\right)e^{2\lambda_{i+1}z}+\frac{\zeta_{i+1}}{\zeta_i}-1}{\frac{B_{i+1}}{C_{i+1}}\left(\frac{\zeta_{i+1}}{\zeta_i}-1\right)e^{2(\lambda_{i+1}+\lambda_i)z}-(\frac{\zeta_{i+1}}{\zeta_i}+1)e^{2\lambda_iz}},\ (1\le i\le N-1). \tag{27}$$

Combining Eq. (25) with Eq. (27), the ratios B_{N-1}/C_{N-1},B_{N-2}/C_{N-2},…, B_2/C_2 and B_1/C_1 in any layer can be explicitly expressed.

From the formula in Eq. (21), the recurrence relationship between C_i and C_{i+1} can be given by:

$$C_{i+1}=C_i\frac{e^{(\lambda_i+\lambda_{i+1})H_i}\frac{B_i}{C_i}+e^{(\lambda_{i+1}-\lambda_i)H_i}}{e^{2\lambda_{i+1}H_i}\frac{B_{i+1}}{C_{i+1}}+1}. \tag{28}$$

Transforming the load boundary at the pile head in Eq. (23) gives the following:

$$C_1=\frac{F_0}{\zeta_1\left(1-\frac{B_1}{C_1}\right)}. \tag{29}$$

Combining Eq. (25) with Eqs. (27)–(29), all the unknown constants can be explicitly solved. The dynamic impedance at the pile head can be obtained from

$$K_d(0)=\frac{-B_1\zeta_1+C_1\zeta_1}{B_1+C_1}. \tag{30}$$

5.2 Attenuation function $\phi(r)$

Collecting the coefficients of $\delta\phi$ from the variational formula in Eq. (12), the following equation can be obtained:

$$\frac{\partial^2\phi}{\partial r^2}+\frac{1}{r}\frac{\partial\phi}{\partial r}-\beta^2\phi=0 \tag{31}$$

where

$$\beta=\sqrt{\frac{n_{s1}-n_{s2}\omega^2}{m_s}} \tag{32}$$

$$m_s=\sum_{i=1}^{M}\int_{H_{i-1}}^{H_i}2\pi G_{si}^{*}w_{pi}^2\mathrm{d}z+\sum_{j=M+1}^{N}\int_{H_{j-1}}^{H_j}2\pi G_{si}^{*}w_{si}^2\mathrm{d}z \tag{33a}$$

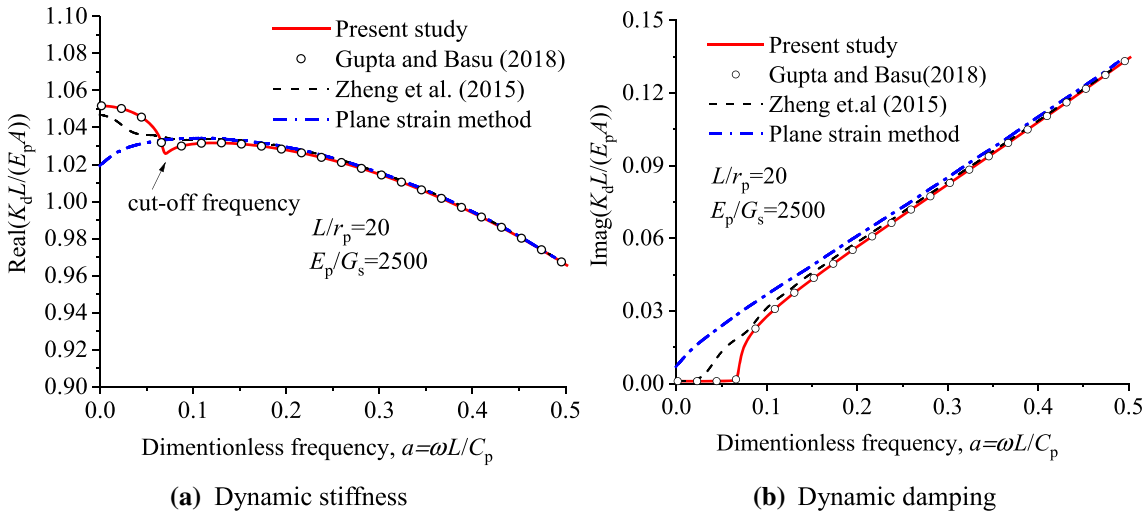

(a) Dynamic stiffness **(b)** Dynamic damping

Fig. 3 Dynamic impedance of piles resting on a rigid base

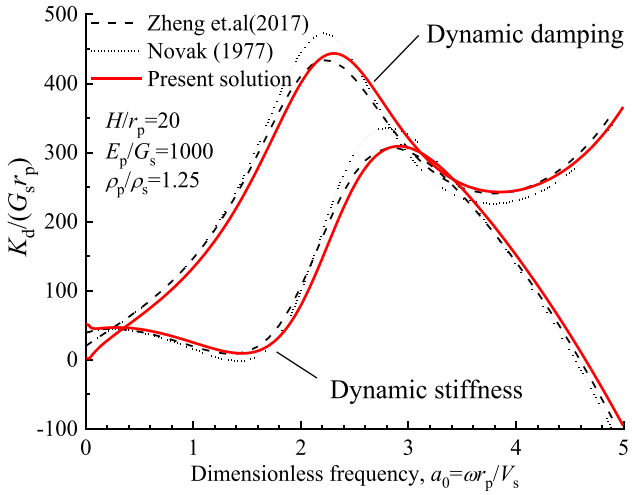

Fig. 4 Dynamic impedance of piles in soil half-space

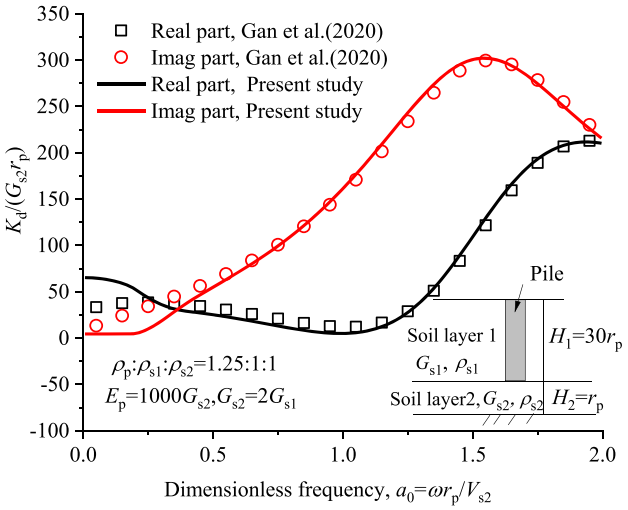

Fig.5 Dynamic impedance of piles in two-layered soil

$$n_{s1}=\sum_{i=1}^{M}\int_{H_{i-1}}^{H_i}\int_{r_p}^{\infty}2\pi\left(\lambda_{si}^{*}+2G_{si}^{*}\right)\left(\frac{\partial w_{pi}}{\partial z}\right)^2\mathrm{d}z + \sum_{j=M+1}^{N}\int_{H_{j-1}}^{H_j}2\pi\left(\lambda_{si}^{*}+2G_{si}^{*}\right)\left(\frac{\partial w_{si}}{\partial z}\right)^2\mathrm{d}z \tag{33b}$$

$$n_{s2}=\sum_{i=1}^{M}\int_{H_{i=1}}^{H_i}2\pi\rho_{si}w_{pi}^2\mathrm{d}z+\sum_{j=M+1}^{N}\int_{H_{j-1}}^{H_j}2\pi\rho_{si}w_{si}^2\mathrm{d}z \tag{33c}$$

By solving Eq. (31), the general solution of $\phi(r)$ is written as:

$$\phi(r)=c_1\mathrm{I}_0(\beta r)+c_2\mathrm{K}_0(\beta r) \tag{34}$$

where I_0 and K_0 are the modified Bessel function of the first and second kinds of zero order, respectively. Given the boundary conditions in Eq. (3), the coefficients c_1 and c_2 in Eq. (34) are determined, which yields:

$$\phi(r)=\frac{K_0(\beta r)}{K_0(\beta r_p)}. \tag{35}$$

Once the displacement decay function is known, the displacement of surrounding soil can be obtained from Eqs. (1) and (18).

6 Solution technique

The pile displacement at any given depth z can be finally expressed by the soil parameters k_i, t_i, α_i, which rely on the displacement decay function ϕ. It is clear that ϕ is determined by other groups of soil parameters m_s, n_{s1}, n_{s2} and β from Eqs. (33a), (33b) and (33c). Consequently, there are

eight undetermined coefficients including k_i,t_i,α_i, m_s, n_{s1}, n_{s2},β and ϕ. These unknown parameters can be determined by solving the corresponding eight equations in Eqs. (32) and (35). Nevertheless, directly solving is not convenient since the undetermined coefficients are intercoupled. An iterative procedure [3, 9, 21, 24] is thus applied to obtain the expected results. First, an initial empirical value of 1.0 is made for the parameter β to calculate the decay function ϕ through Eq. (35). Then, the other six undetermined coefficients can be instantly calculated through Eqs. (15), (33). In detail, the values of k_i,t_i,α_i can be determined through Eqs. (15a), (15b) and (15c). The pile displacement subsequently can be obtained through Eqs. (18), (27) and (28). After calculating m_s, n_{s1}, n_{s2} through Eqs. (33a), (33b), (33c), the value of β can be updated by Eq. (32). Repeating the entire process until the tolerance between the new and old value of β is less than 10^{-3}. Finally, the pile-head dynamic impedance can be calculated through Eq. (30).

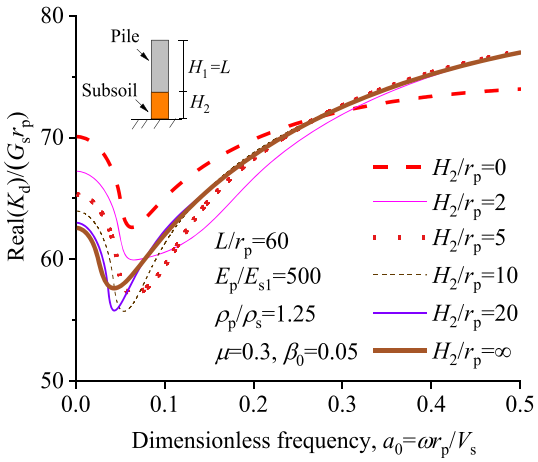

(a) Dynamic stiffness

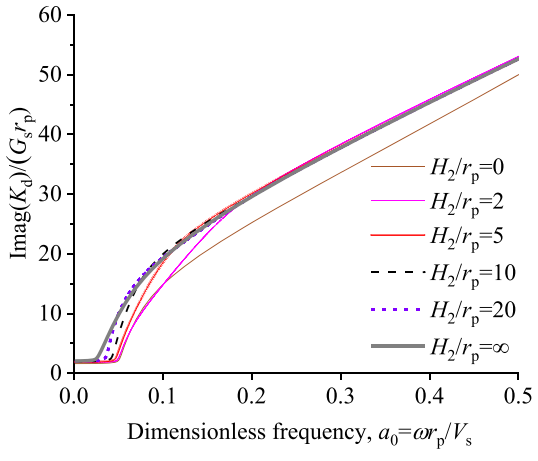

(b) Dynamic damping

Fig. 6 Variation of dynamic impedance K_d versus dimensionless frequency a_0 for different thickness of the lower soil layer

7 Comparison and validation with existing analytical solutions

By modifying the soil profile and corresponding mechanical properties, the present solution is capable to analyze the dynamic responses of the vertically loaded pile in various geotechnical cases. In Fig. 3, the present solution is compared with the analytical results for the dynamic impedance of end-bearing piles obtained by Gupta and Basu [3], Zheng et al. [28] and Novak's plane strain method. In this case, the slender ratio of the pile is $L/r_p = 20$, and the other parameters are: $E_p/G_s = 2500$, $\beta_0 = 0.02$, $\rho_s = 2200$ kg/m^3, $\rho_p = 2500$ kg/m^3, $\upsilon_s = 0.3$. To apply the present model, the soil profile contains two layers: The soil parameters of the upper one are the same with those in the previously published solutions, whereas the soil modulus of the lower soil layer is set $10^4 G_s$ to simulate the rigid rock base. Figure 3 shows that the present solution agrees well with Gupta and Basu [3], which is anticipated since their deduction also restricted the radial displacement in soil. Zheng et al. [28] relaxed that restriction and obtained a rigorous analytical solution that is eligible to capture two cut-off frequencies. Novak's plane strain method neglected the vertical stress gradient in soil and thus can only consider the horizontal wave propagation in soil. Figure 3 reveals that Novak's method overestimates the dynamic damping and underestimates the dynamic stiffness in low frequency range of $0 < a_0 < 0.1$. Compared with the existing methods, the present solution could produce one cut-off frequency, and the accuracy of dynamic impedance is overall acceptable.

Figure 4 compares the curves of dynamic pile-head impedance versus frequency in half soil-space. Note that that the impedance K_d is nondimensionalized as $K_d/(G_s r_p)$ and frequency ω is nondimensionalized as $\omega r_p/V_s$, where G_s and V_s denote the shear modulus and the speed of shear wave in the first soil layer. To apply the present model, the soil profile contains two layers with identical parameters, whereas the depth of the lower soil layer is set $40L$ to simulate the half soil-space. Compared with this present solution, Zheng et al. [29] and Novak [14] solution both predict a slightly smaller dynamic stiffness and larger dynamic damping in low frequency range less than 0.1, which owes that they treat the surrounding soil as independent thin layers, and thus, the pile–soil system becomes more flexible than the actual condition at low frequencies. As frequency increases, the waves in soil tend to propagate in a horizontal manner and the energy transfer between

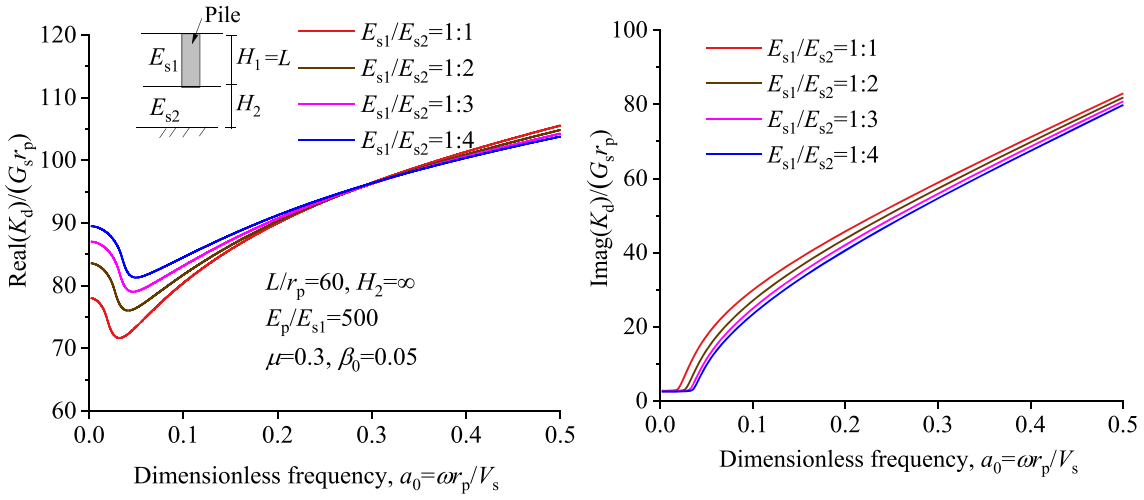

(a) Dynamic stiffness, L/r_p=60 **(b)** Dynamic damping, L/r_p=60

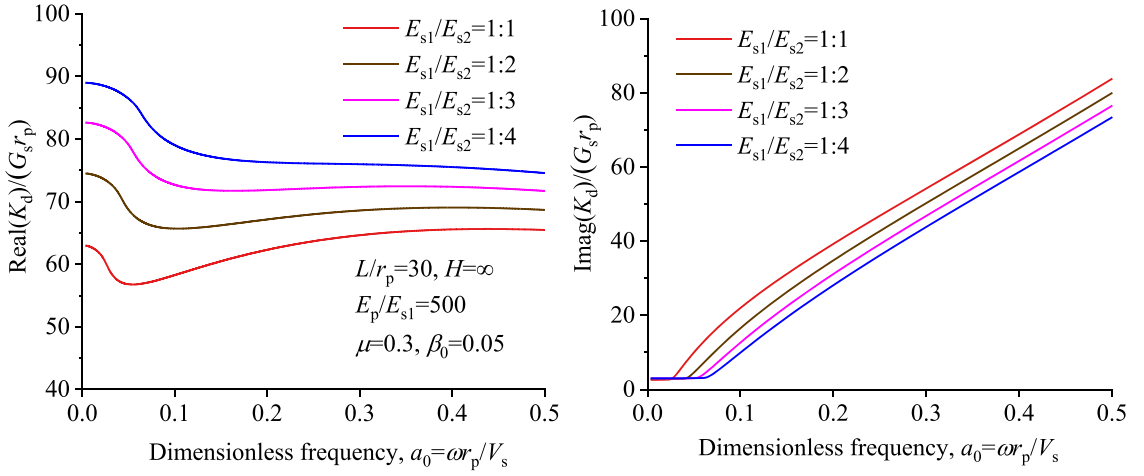

(c) Dynamic stiffness, L/r_p=30 **(d)** Dynamic damping, L/r_p=30

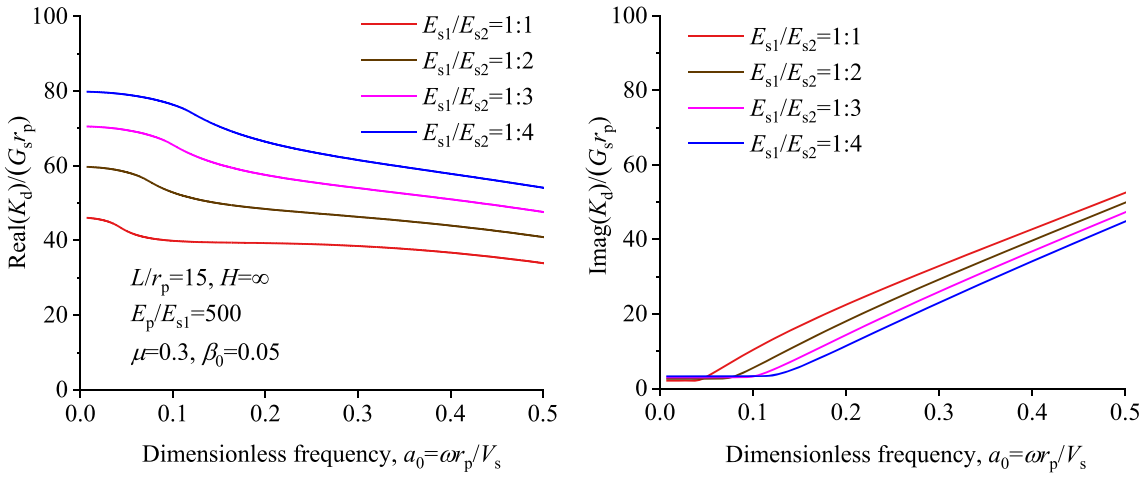

(e) Dynamic stiffness, L/r_p=15 **(f)** Dynamic damping, L/r_p=15

Fig. 7 Variation of dynamic impedance K_d versus dimensionless frequency a_0 for different Young's modulus of the lower soil layer

adjacent soil layers becomes less significant [12, 13]. Unsurprisingly, the dynamic stiffness calculated by this present solution and Zheng et al.'s method [29] could make a better match as excitation frequency grows. Besides, Novak [14] overestimates the dynamic impedance at resonance frequencies because it fails to account for the infinite nature of soil half-space by modeling the soil beneath the pile tip as Winkler springs and damping dashpots.

Furthermore, in Fig. 5, a comparison of the dynamic pile-head impedance in a two-layered ground from this present solution is performed with the results in Gan et al. [6], where elastodynamic theory and the method of Hankel transformation are employed to produce the analytical solutions of vibrating pile in two layers. The results show that the pile impedances calculated by this present study and Gan et al. [6] agree very well for $a > 0.3$. Mild difference occurs at a low frequency range of $0 < a < 0.3$, which is due to the independent thin layers assumption for surrounding soil in Gan et al. [6].

8 Results and discussion

8.1 Influence of substrtum on pile-head dynamic impedance

8.1.1 The thickness of substrtum

Figure 6 shows the dynamic impedance variation of piles supporting by soil layers with various thickness H_2. The soil profile is assumed homogenous, and pile length remains unchanged in this section. H_2 is chosen to range from 0 to ∞, which means the pile tip condition varies from end-bearing to infinite half soil-space. The results show that the static impedance ($a_0 = 0$) falls with a decreasing rate as H_2 increases in Fig. 6a. The static impedance for the case at end-bearing condition is around 14% greater than that at infinite half soil-space condition. As frequency grows from $a_0 = 1$ to $a_0 = 0.5$, the dynamic impedance gradually decreases before cut-off frequency occurs and then continuously increases until the end. The cut-off frequency slightly decreases with H_2 increases, whereas the minimum values of dynamic impedance decrease from $H_2 = 0$ to $H_2 = 10r_p$ and then behave a relatively slow growth as H_2 becomes greater. Figure 6b shows a clear variation of cut-off frequency versus H_2. Besides, the dynamic damping for the case of $H_2 = 2r_p$ tends to coincide with that of $H_2 = \infty$ as a_0 exceeds a threshold value around 0.18; for the cases of $H_2 = 5r_p$, $H_2 = 10r_p$ and $H_2 = 20r_p$ that threshold values decrease to around 0.1, 0.6 and 0.4. The falling process of threshold value reflects that the curves of dynamic impedance against frequency move toward the case in infinite half soil-space as H_2 continuously increases.

8.1.2 Influence of Young's modulus of the lower soil layer

Figure 7 depicts the variation of dynamic pile-head impedance as substratum modulus varies. The thickness of substratum in this section is considered as infinite, and the modulus of the upper soil layer remains constant. The results show that increasing substratum modulus evidently increases the dynamic stiffness before cut-off frequency in Fig. 7a. An increase of four times on substratum modulus brings around 17% growth of dynamic stiffness before cut-off frequency. That growth gradually becomes smaller as frequency increases. Because the dynamic stiffness in

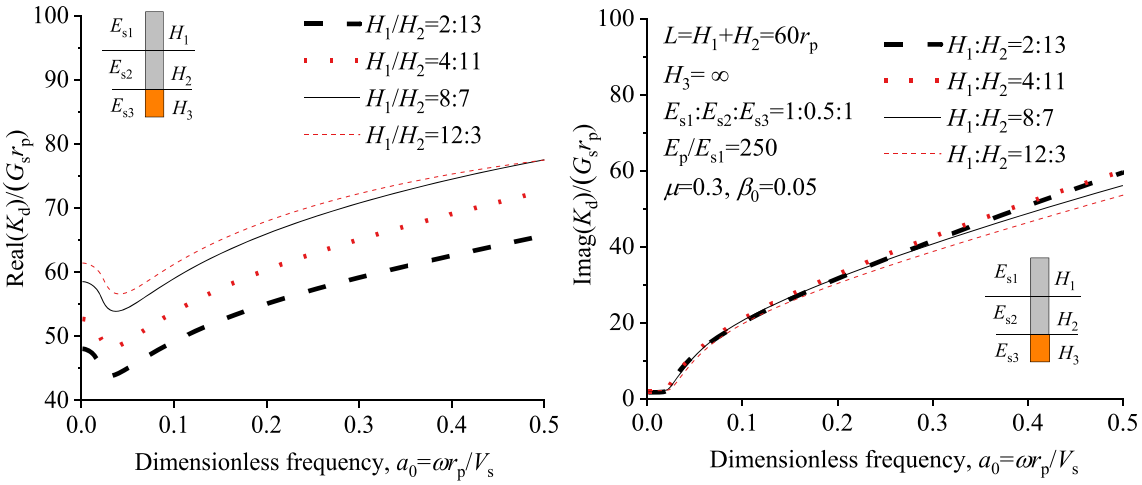

(a) Dynamic stiffness **(b)** Dynamic damping

Fig. 8 Variation of dynamic impedance K_d versus dimensionless frequency a_0 for different thicknesses of the middle soil layer

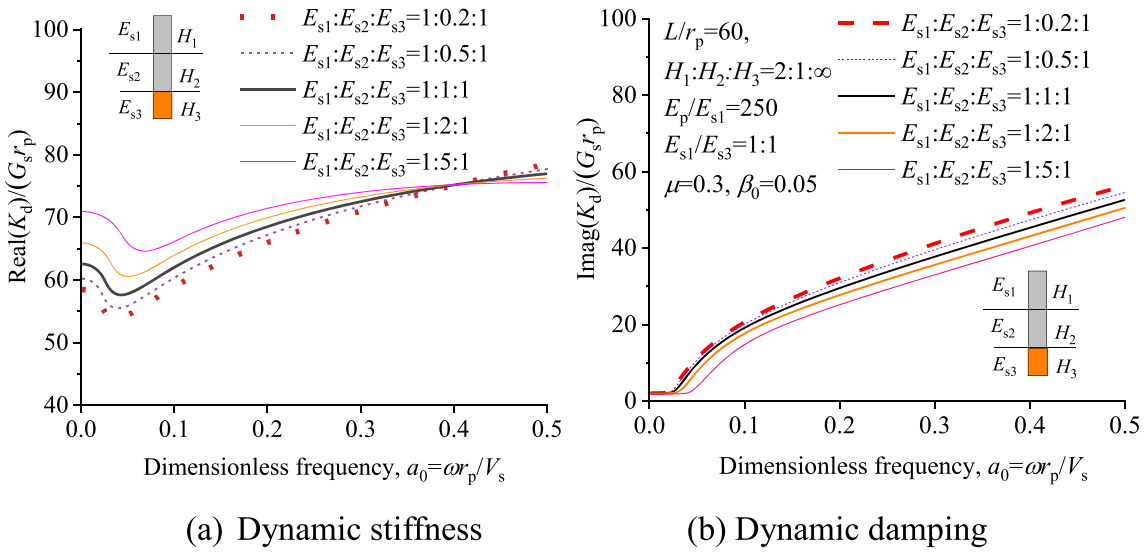

Fig. 9 Variation of K_d versus dimensionless frequency a_0 for different Young's modulus of the middle soil layer

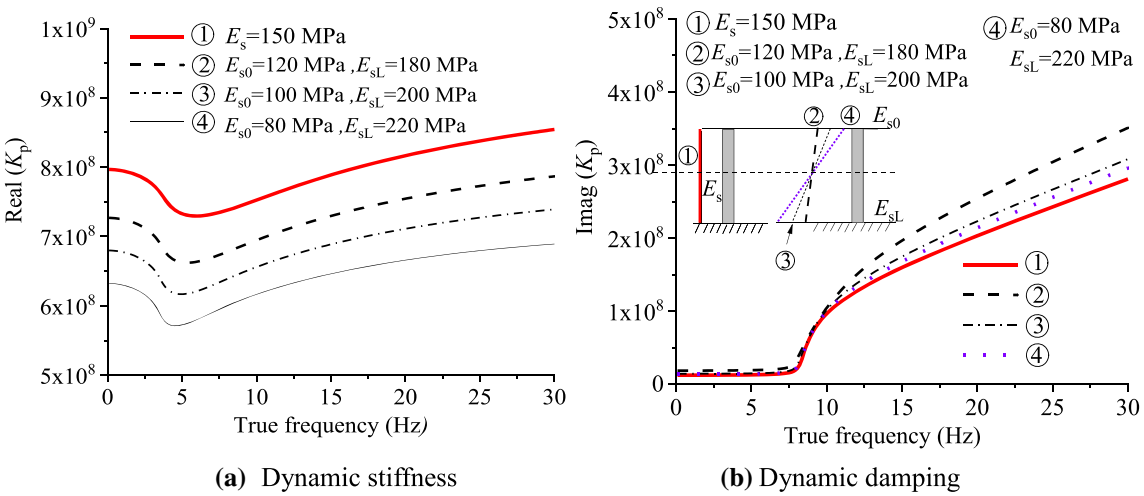

Fig. 10 Variation of dynamic impedance versus true frequency as the modulus of Gibson soil varies (L = 25 m, r_p = 0.25 m, E_p = 25GPa, ρ_p/ρ_s = 1.25, μ_s = 0.3)

weaker substratum increases relatively faster than that in stiffer one, it appears that the curves of dynamic stiffness versus frequency coincide at around a_0 = 0.3. After that, the dynamic stiffness in weaker substratum tends to exceed that in the stiffer counterpart. In Fig. 7b, it is found that the curves of dynamic damping versus frequency are approximately parallel for four types of substratum modulus. The weaker substratum modulus causes greater dynamic damping, whereas that difference is generally limited.

Figure 7c, e shows the dynamic stiffness of piles as substratum modulus varies for cases of pile slender ratio L/r_p = 30 and L/r_p = 15, respectively. The results show that increasing substratum modulus brings in a more significant increase for dynamic stiffness as L/r_p decreases. Increasing substratum modulus to four times produces around 43% growth for the static stiffness when L/r_p = 30, and that growth is around 76% when L/r_p = 30. That phenomenon is understandable since a greater portion of the load is transferred to the substratum in the piles with a greater pile slender ratio. Besides, the dynamic stiffness reduction around cut-off frequency is less prominent as L/r_p increases. A significant difference in dynamic stiffness occurs with the variation of substratum modulus in the given frequency range $0 < a_0 < 0.5$.

Figure 7d, f shows the corresponding dynamic damping of Fig. 7c, e, respectively. It is observed that the dynamic damping tends to decrease, and substratum modulus exerts a greater influence as L/r_p increases.

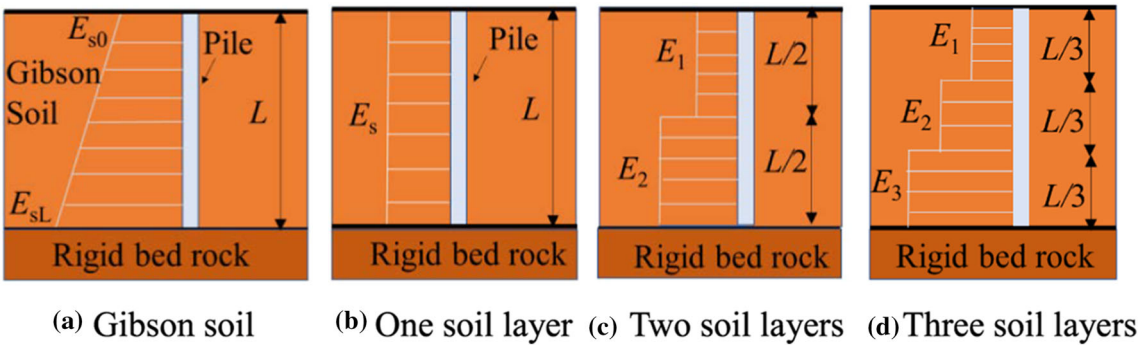

Fig. 11 Illustration of end-bearing piles in Gibson soil and its equivalent layered soil on rigid bed rock, E_{s0}:E_{sL} = 1:4

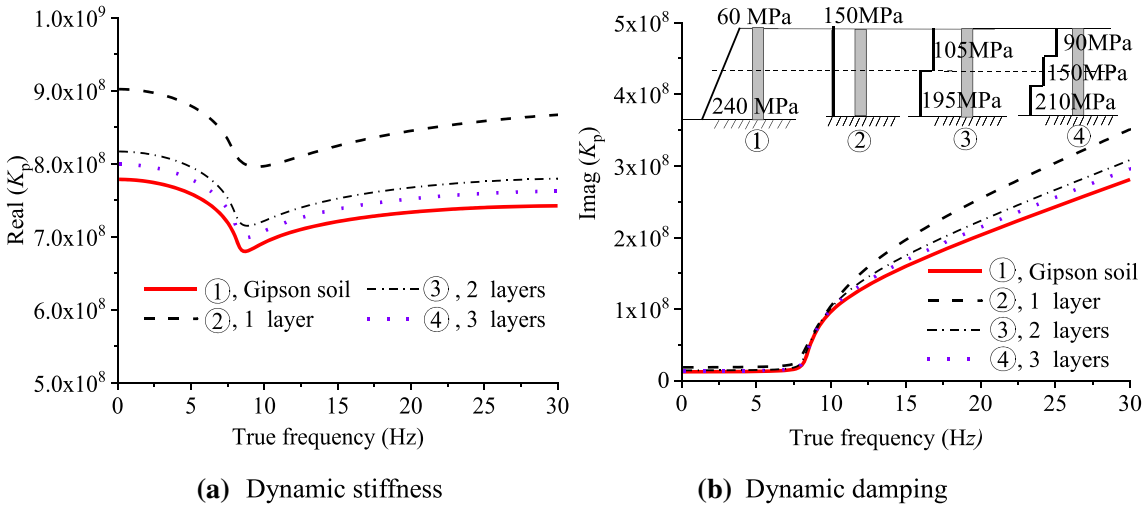

Fig. 12 Comparison of the dynamic impedance of end-bearing piles in Gibson soil and equivalently homogeneous layered soil. L = 10 m, r_p = 0.25 m, E_p = 25 GPa, ρ_p/ρ_s = 1.25, μ_s = 0.3

8.2 Influence of lateral interlayer on pile-head dynamic impedance

In this section, the soil profile contains three layers with two layers surrounding the pile and one below the pile. The lateral interlayer is set as the second or the middle one. Note that the third layer is extended to the infinite and the pile length is constant.

8.2.1 Influence of the thickness of the lateral interlayer

Figure 8 shows the variation of dynamic impedance as the thickness of the middle layer H_2 varies. The Young's modulus of middle layer E_{s2} is assumed to be half of E_{s1} and E_{s3}. The results show that dynamic stiffness increases when the middle soft layer becomes thinner in Fig. 8a. A growth of around 21% for dynamic stiffness is observed at the given frequency range ($0 < a_0 < 0.5$) as H_1:H_2 decreases from 12:3 to 2:13. Figure 8b shows that dynamic damping slightly increases as the weak interlayer becomes thicker, whereas the influence of weak interlayer is not significant when the frequency is relatively low or $a_0 < 0.3$. Moreover, Fig. 8 demonstrates that the cut-off frequency of dynamic impedance is barely affected by the thickness ratio of H_1/H_2.

8.2.2 Influence of Young's modulus of lateral interlayer

In this part, the thickness of the middle layer remains the same, but Young's modulus varies. Figure 9 reflects that the value of cut-off frequency controls the variation of dynamic impedance. In Fig. 9a, it is shown that the influence of the interlayer modulus also relies on the frequency: When $a_0 < a_{\text{cut-off}}$, the reduction of dynamic stiffness induced by weak interlayer has a limited variation with frequency; when $a_0 > a_{\text{cut-off}}$, that reduction gradually turn down with frequency increases. As the frequency continues to increase to $a_0 > 0.4$, the dynamic stiffness for the weaker middle layer case tends to be greater than that for the stiffer middle layer case. In Fig. 9b, it is shown that the influence of interlayer modulus on dynamic damping slightly intensifies as frequency increases. At a_0 = 0.1, and

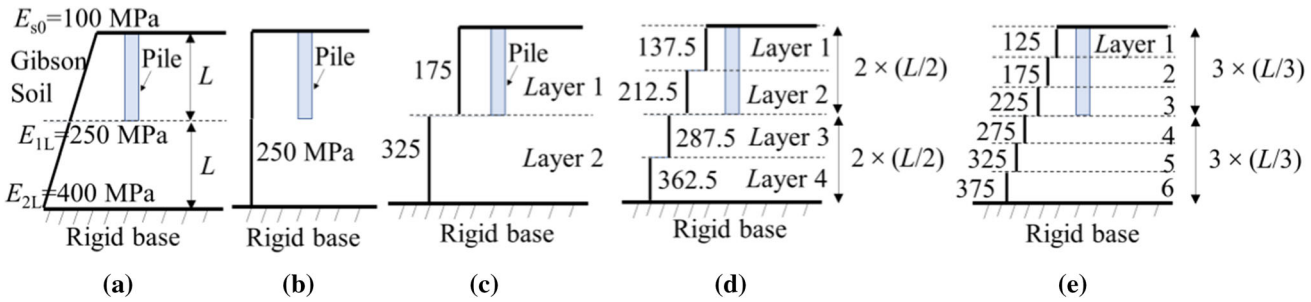

Fig. 13 Illustration of floating piles in Gibson soil and its equivalent layered soil: **a** Gibson soil; **b** one soil layer for the whole soil domain; **c** one layer for lateral soil and pile tip soil, respectively; **d** two layers for lateral soil and pile tip soil, respectively; **e** three layers for lateral soil and pile tip soil, respectively

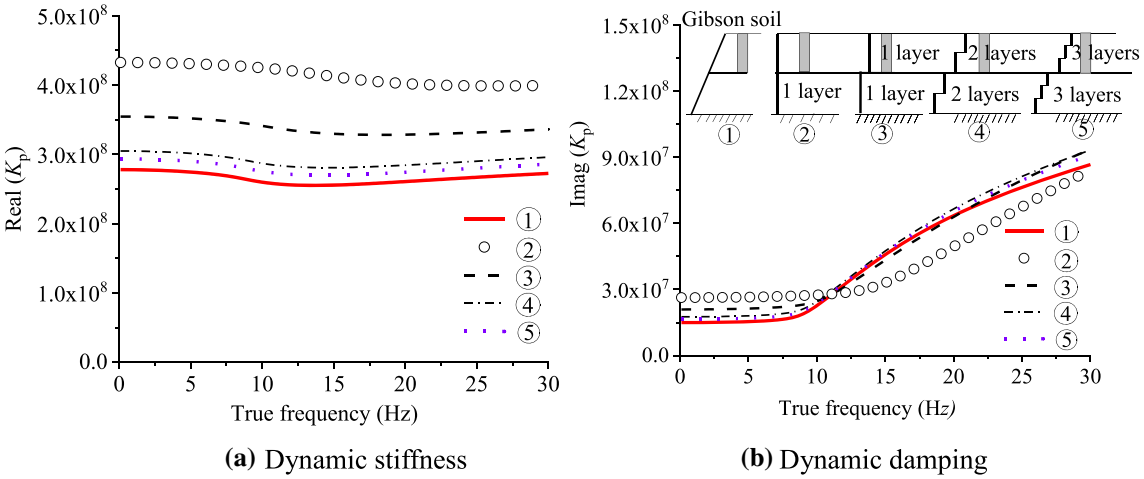

Fig. 14 Comparison of the dynamic impedance of piles in Gibson soil and equivalently homogeneous layered soil. L = 10 m, r_p = 0.1 m, E_p = 25GPa, ρ_p/ρ_s = 1.25, μ_s = 0.3

a_0 = 0.5, the corresponding reduction of dynamic damping is around 5% and 10%, respectively.

8.3 Influence of Gibson-type soil on pile-head dynamic impedance

For natural sedimentary ground, the modulus of soil is often depth-dependent. Here, we consider the case of Gibson soil, i.e., the soil modulus linearly increases with the depth from E_{s0} to E_{sL}. To calculate the dynamic impedance using the presented solution, the Gibson soil is treated as infinite soil layers. The influences of Gibson soil on the dynamic impedance are investigated for the end-bearing and floating piles, respectively.

8.3.1 Dynamic impedance of end-bearing piles

Figure 10 depicts the dynamic impedance of end-bearing piles in Gibson soil. The results show that the pile-head dynamic stiffness increases as the surface modulus increases. Moreover, the dynamic stiffness of piles in Gibson soil is prominently smaller than that in the homogeneous soil with a modulus of $(E_{s0} + E_{sL})/2$ in a given frequency range. Dynamic stiffness in case ④ is 26% smaller than that in case ①. That phenomenon owes that the surface modulus in Gibson soil is larger than that in the corresponding homogeneous soil. Besides, a relatively small variation of the curve shape of dynamic stiffness versus frequency is observed for the cases ①, ②, ③ and ④. Furthermore, it appears that the cut-off frequency of pile impedance is insensitive to the variation of surface modulus in Gibson soil on the condition that the average modulus remains constant.

To make a convenient approximation on pile behaviors, a common approach is to treat the inhomogeneous soil profile as equivalently layered soil as shown in Fig. 11. When representing the ground with one homogeneous soil layer, the equivalent modulus is calculated by $(E_{s0} + E_{sL})/2$. When representing the ground with two soil layers, the equivalently homogenized modulus of the upper layer can be written as $(E_{s0} + (E_{s0} + E_{sL}))/2$, because the actual modulus of the upper layer varies from E_{s0} to $(E_{s0} + E_{sL})/2$. Similarly, the equivalent modulus of the lower soil layer is given by $(E_{sL} + (E_{s0} + E_{sL}))/2$.

Figure 12 shows that the effects of the equivalent soil layer numbers on the dynamic impedance of piles in Gibson soil. The ratio of surface modulus and bottom modulus is 1:4. The results show that the equivalently homogeneous approach could give approximately close cut-off frequency for the pile-head impedance in Gibson-type soil. Furthermore, the one-layer approach produces a deviation of 15% for dynamic stiffness; the two-layer approach produces a much better result with a deviation of 5%; and the deviation decreases to less 3% for the three-layer approach. The above comparison demonstrates that replacing Gibson soil with two or more layers with equivalent modulus can predict the dynamic impedance with acceptable accuracy for engineering design.

8.3.2 Dynamic impedance of floating piles

For the cases of floating piles in Gibson soil (see Fig. 13a), four types of equivalent layered soil are illustrated in Fig. 13b–e. The soil profile in Fig. 13b treats the Gibson soil as a homogeneous ground, and the corresponding equivalent soil modulus is the average of surface modulus E_{s0} and bottom modulus E_{2L}. In Fig. 13c, the lateral soil ($0 \leq H < L$) and pile tip soil ($L \leq H < 2L$) are treated as a homogeneous soil layer with Young's modulus of 175 MPa and 325 MPa, respectively. Similar treatment with that in Fig. 11 is employed to the lateral soil and pile tip soil, respectively, to produce equivalently homogeneus soil profiles with one layer, two layers and three layers as illustrated in Fig. 13c–e.

Figure 14 compares the vertical dynamic impedance of the piles in Gibson soil and aforementioned four types of equivalently homogeneous layered soil. The results show that equivalent soil ② brings an overestimation of around 56% for dynamic stiffness. That overestimation decreases to around 26% when the lateral soil and pile tip soil are separately treated as one homogeneous layer (case ③). It appears that one equivalent layer approach induces more prominent deviation of dynamic impedance for floating piles than end-bearing piles in Gibson soil. Moreover, increasing the number of layers to two and three overestimates the pile-head dynamic stiffness up to around 10% and 6%, respectively. Good agreement also can be found for the curves of dynamic damping against frequency when increasing the number of equivalent soil layers.

9 Conclusions

A novel close-form solution is developed to obtain the dynamic responses of axially loaded piles in inhomogeneous soil by applying Hamilton's energy principle. Viscoelastic property is attributed to soil domain and its displacement field is formulated as the product of pile displacement and decay function. The soil column beneath the pile tip is considered as a fictitious soil pile to implement the displacement description for the whole pile–soil continuum system. This present model is capable to obtain the responses of longitudinal vibrating pile in various horizontal ground profiles —homogeneous, layered and Gibson soil. Additionally, it can distinguish the effects of material damping and radical damping and thus gives a satisfactory prediction for dynamic impedance at low frequencies. The conclusions can be drawn as follows:

1. The influence of substratum modulus and thickness on dynamic stiffness depends on the cut-off frequency. When $0 < a < a_{\text{cut-off}}$, the dynamic stiffness generally decreases as frequency increases, and the piles with thicker and weaker substratum layers undergo a more significant reduction of dynamic stiffness. When $a > a_{\text{cut-off}}$, the difference of dynamic stiffness induced by the substratum layer tends to decrease as frequency increases.
2. The influences of substratum on dynamic impedance are highly associated with the pile geometry. Especially, the piles with short and stubby shape undergo a more significant variation of dynamic impedance than that with a long and slim shape.
3. The thickness variation of the surrounding interlayer soil generally causes more significant influences on the dynamic stiffness than the modulus variation in given cases.
4. The dynamic stiffness of piles in Gibson soil is more sensitive to the surface modulus than the bottom modulus. Representing the Gibson soil with one homogeneous soil layer produces more remarkable overestimation for the dynamic stiffness of floating piles than end-bearing piles. As the number of equivalent soil layers increases, the deviation of pile dynamic stiffness in layered soil and Gibson type dramatically decreases.

Acknowledgements This research was financially supported by National Natural Science Foundation Project (No: 52078426); National Key Research and Development Plan (No. 2018YFE0207100); 2018 Sichuan province Ten thousand people plan.

References

1. Cui CY, Zhang S, Chapman D et al (2018) Dynamic impedance of a floating pile embedded in poro-visco-elastic soils subjected to vertical harmonic loads. Geomech Eng 15(2):793–803
2. Cristina M, Juan A, Luis P et al (2013) Effects of soil–structure interaction on the dynamic properties and seismic response of piled structures. Soil Dyn Earthq Eng 53:160–175

3. Gupta BK, Basu D (2018) Dynamic analysis of axially loaded end-bearing pile in a homogeneous viscoelastic soil. Soil Dyn Earthq Eng 111:31–40
4. Goit CS, Saitoh M, Igarashi T et al (2020) Inclined single piles under vertical loadings in cohesionless soil. Acta Geotech. https://doi.org/10.1007/s11440-020-01074-9
5. Gazetas G, Fan K, Kaynia A (1993) Dynamic response of pile groups with different configurations. Soil Dyn Earthq Eng 12:239–257
6. Gan SS, Zheng CJ, Kouretzis G et al (2020) Vertical vibration of piles in viscoelastic non-uniform soil overlying a rigid base. Acta Geotech 15:1321–1330
7. Kouroussis G, Anastasopoulos I, Gazetas G, et al (2013) Three-dimensional finite element modelling of dynamic pile-soil-pile interaction in time domain. In: Proceedings of 4th ECCOMAS thematic conference. Kos Island, Greece
8. Kanellopoulos K, Gazetas G (2020) Vertical static and dynamic pile-to-pile interaction in non-linear soil. Géotechnique 70(2):432–447
9. Lee KM, Xiao ZR (1999) A new analytical model for settlement analysis of a single pile in multi-layered soil. Soils Found 39(5):131–143
10. Liu HL, Wang CL, Kong GQ et al (2019) A simplified design method for energy piles. Acta Geotech 14(3):1–9
11. Li ZY, Gao YF (2019) Effects of inner soil on the vertical dynamic response of a pipe pile embedded in inhomogeneous soil. J Sound Vib 439:129–143
12. Makris N, Gazetas G (1993) Displacement phase differences in a harmonically oscillating pile. Géotechnique 43(1):135–150
13. Mylonakis G, Gazetas G (1998) Vertical vibration and additional distress of grouped piles in layerd soil. Soils Found 38(1):1–14
14. Novak M (1977) Vertical vibration of floating piles. J Eng Mech Div ASCE 103:153–168
15. Novak M (1974) Dynamic stiffness and damping of piles. Can Geotech J 4:574–598
16. Poulos HG (2005) Pile behaviors-consequences of geological and construction imperfections. J Geotech Geoenviron Eng 131(5):538–563
17. Peng Y, Liu HL, Li C et al (2021) The detailed particle breakage around the pile in coral sand. Acta Geotech. https://doi.org/10.1007/s11440-020-01089-2
18. Qu LM, Ding XM, Kouroussis G et al (2021) Dynamic interaction of soil and end-bearing piles in sloping ground: numerical simulation and analytical solution. Comput Geotech. https://doi.org/10.1016/j.compgeo.2020.103917
19. Qu LM, Ding XM, Zheng CJ et al (2017) An analytical solution for wave propagation in a square pile due to transient point load. Comput Geotech 83:77–82
20. Qu LM, Ding XM, Zheng CJ, Wu CR, Cao GW (2021) Vertical vibration characteristics of group piles in sloping topography. Earthq Eng Eng Vib 20(2):377–390
21. Seo H, Prezzi M (2007) Analytical solutions for a vertically loaded pile in multilayered soil. Geomech Geoeng Int J 2(1):51–60
22. Salgado R, Seo H, Prezzi M (2013) Variational elastic solution for axially loaded piles in multilayered soil. Int J Numer Anal Methods Geomech 37(4):423–440
23. Ullah MS, Yamamoto H, Goit CS et al (2018) On the verification of superposition method of kinematic interaction and inertial interaction in dynamic response of soil-pile-structure systems. Soil Dyn Earthq Eng 113:522–533
24. Vallabhan CVG, Mustafa G (1996) A new model for the analysis of settlement of drilled piers. Int J Numer Anal Methods Geomech 20:143–152
25. Wu WB, Jiang GS, Huang S et al (2014) Vertical dynamic response of pile embedded in layered transversely isotropic soil. Math Probl Eng 12:1–12
26. Wu WB, El Naggar MH, Abdlrahem M et al (2017) New interaction model for vertical dynamic response of pipe piles considering soil plug effect. Can Geotech J 54:987–1001
27. Wu JT, Wang KH, Liu G et al (2019) Study on longitudinal vibration of a pile with variable sectional acoustic impedance by integral transformation. Acta Geotech 14:1857–1870
28. Zheng CJ, Ding XM, Li P et al (2015) Vertical impedance of an end-bearing pile in viscoelastic soil. Int J Numer Anal Methods Geomech 39:676–684
29. Zheng CJ, Gan SS, Ding XM et al (2017) Dynamic response of a pile embedded in elastic half space subjected to harmonic vertical loading. Acta Mech Solida Sin 30(6):668–673